한국지반공학회논문집 제17권 제2호 2001년 4월 PP. 135 ~ 142

Application of Porous Medium Theory in Slope Stability Analysis

다공체 이론을 사용한 사면안정해석

Seo, Young-Kyo* 서 영 교

요 지

사면안정해석을 위해 다공체(porous medium) 이론이 제시되었다. 다공체 이론은 간극수압, 토질입자 및 간극수의 상호작용을 포함하는 여러 가지 지반관련 문제의 이해에 있어 매우 중요하다. 이러한 상호작용은 토질강도 및 변형에 중요한 영향을 미친다. 압밀 예제로서 이러한 모델의 정확도를 첫째로 검증하였다. 사면안정해석에 있어서 토질의 응력 및 강도는 일반적인 구성모델을 포함한 비선형 유한요소해석을 사용하여 정확히 계산되었다. 사면안정해석은 한계상태를 표시하는 파괴면이 나타날 때까지 점차적인 중력의 증가로 실행되었다. 안전율은 증가시킨 중력과 실제사면 중력의 비로서 계산되었다. 제시된 사면 안정 해석 방법의 자세한 사항은 예제를 통하여 설명되었다.

Abstract

The porous medium theory is introduced for computing the stability analysis of slopes. Such models are important for many geotechnical problems due to relavant interaction between interstitial pore fluid and soil skeleton, which can have significant effects on soil strength behaviors. Consolidation example demonstrated the accuracy of the numerical model. In the slope stability analysis, the soil stresses and strengths are computed accurately using inelastic finite element methods with general constitutive models. In the slope analysis procedures, the gravitational loading on the slope monotonically increases until the critical limit state instability mechanisms are developed. Slope stability factors are represented as the ratio of load magnitude which first generates instability of the slope to the magnitude of the expected load. Further discussions are explained along with the solved examples.

Keywords : Porous media model, Slope stability analysis, Finite element method, Soil plasticity model, Limit state analysis

1. Introduction

Porous materials such as soils consist of a solid skeleton and voids or porosity which can contains various fluid and air. When loads are applied to the porous medium, there is an interaction between the deformation of the soil skeleton and fluid flow. Such theories were first developed by Terzaghi(1950) and Biot(1962) for linear elastic and linear visco-elastic porous materials. Some applications of the finite element method to the theory of elasto-plastic mixtures have been reported. Among them, Prevost(1980) and Borja(1986) developed the velocity (pressure)-displacement formulation of fluid saturated soil mixtures. While both formulations have their own advantages, a porous medium treatment with a velocity formulation is utilized in this work since it leads to homogeneous systems of finite element equations. Whereas the preceding works(Smith, 1976) have utilized multi-phase continuum/FEM models to

* 정회원, 부산대학교 전임연구원

compute consolidation settlements of embankments without concern for possible shear failure of the soil system.

The intention of this work is the application of porous theory for the slope on saturated soil deposits. Using classical methods and assumptions, the stability analysis of such systems typically proceeds by assuming that the saturated soil has a response behavior that is either no-flow(fully undrained) or free-flow(fully drained) as special cases of porous medium. Since the computed stability factors associated with these assumptions are generally not close in value, the classical methods can leave considerable uncertainty directly attributable to rate dependent pore pressure diffusion effects. Methods of slope stability analysis are thus needed to take into account with the time scale and spatial distribution of pore pressure diffusion occurring in the underlying saturated soil deposit. The objective of this paper is therefore to extend the preceding gravity increase finite element method for stability analysis of earthen slope which was presented in Swan and Seo(1999) using only total stress analysis, to account for pore pressure effects using a coupled pore-pressure and effective stress analysis.

While the proposed framework for slope/embankment /dam stability analysis generally can be employed with a wide variety of soil models, the smooth elasto-plastic cap model is employed in this work. The attractive aspects of the cap model are its continuous and differentiable coupling between shear strength and compressibility behaviors. The details of cap models and the slope stability analysis procedure will be described in the following.

2. Theory of Porous Medium

2.1 Field Equations

The treatment of soils to be employed here is that of a porous, granular solid skeletal continuum interacting with a continuous pore fluid. For clarity and completeness of the slope stability analysis framework, the basic mass and momentum balance equations for both fluid and solid phases of the soil are briefly developed below. A more extensive development of these equations can be found in Provest (1980). In the following, the average intrinsic micro densities of both the fluid and solid phases are denoted by ρ_α ,where $\alpha = w$ denotes the fluid phase and $\alpha = s$ the solid phase. In a representative volume element of soil, the respective volume fractions of the fluid and solid grain phases are denoted by n^w and n^s. Accordingly, macroscopicmass densities of the fluid and solid phases are denoted by ρ^w and ρ^s, and are related to the intrinsic average micro densities as follows

$$\rho^w = n^w \rho_w \qquad \rho^s = n^s \rho_s \tag{1}$$

The continuum mechanics sign convention is used in this work and so stresses and strains are positive in tension and negative in compression. Fluid pressures, however, are taken as positive in compression. With this sign convention, the balance of linear momentum equations for the fluid and solid phases can be expressed in general form as

$$\nabla \cdot \sigma^\alpha + \hat{p}^\alpha = \rho^\alpha (a^\alpha - b) \tag{2}$$

where $\hat{p}^\alpha$ is a momentum supply to the α^{th} constituent from the rest of the mixture due to interaction effects, and b is a body force per unit mass. Momentum transfer between the solid skeleton and the pore fluid is assumed to consist of diffusive and dilatational contributions as follows

$$\hat{p}^s = - \hat{p}^w = - \xi \cdot (v^s - v^w) - p_w \nabla n^w \tag{3}$$

where ξ is the soils' resistivity tensor which is merely the inverse of its symmetric, positive definite permeability tensor. In general momentum balance equations (2), the partial stress tensor σ^w for the pore fluid is simply

$$\sigma^w = n^w \sigma_w = - n^w p_w 1 \tag{4}$$

where p_w represents an average pore fluid pressure on the microscale, and 1 is the identity tensor. In a similar fashion, the mathematical expression for the partial stress tensor of the solid phase σ^s is

$$\sigma^s = n^s \sigma_s \tag{5}$$

where σ_s represents an average solid stress state in the soil

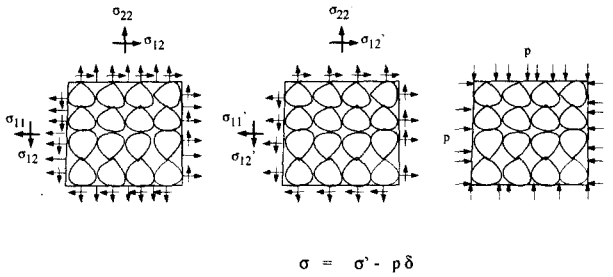

Fig.1. Total and effective stresses in porous medium

on the microscale. The partial solid stress σ^s is not to be confused with Terzaghi's effective stress σ' (Terzaghi, 1927), although the relationship between the two is straightforward for the most soil. For example, the total average stress on a planar segment passing through a sequence of vanishingly small grain-to-grain contact areas can be written as

$$\sigma = \sigma^s + \sigma^w = \sigma' - p_w 1 \tag{6}$$

Figure 1 shows the total and effective stresses in the porous media.

When these notations mentioned above are employed in equation (2), and convective inertial term are neglected and under quasi-static conditions then specific linear momentum equations for both the skeleton and the pore fluid reduced to

$$\nabla \cdot (\sigma' - n^s p_w 1) - \xi \cdot (v^s - v^w) + \rho^s b = 0 \tag{7}$$

$$-\nabla (n^w p_w) + \xi \cdot (v^s - v^{w)} + \rho^w b = 0 \tag{8}$$

2.2 Finite Element Formulation

In the following, the response of soils subjected to gravitational loading will be treated as general materially nonlinear parabolic initial boundary value problems in which the governing field equations are those provided in (7) and (8). With seepage and pore pressure effects included in these field equations, the analysis problems to be solved will feature physically based time dependence. Introducing appropriate initial and boundary conditions, and usage of a Galerkin weighted residual formulation in which the real and variational kinematic fields are expanded in terms of the same nodal basis functions, and discretization of the time domain into a finite number of discrete time points, leads to the following force balance equations at each unrestrained node A in the mesh of the soil domain as here at the $(n+1)^{th}$ time step:

$$(r_A)_{n+1} = (f_A^i)_{n+1} - (f_A^e)_{n+1} = 0 \tag{9}$$

where

$$(f_A^i)_{n+1} = \begin{bmatrix} \int B_A^T (\sigma' - n^s p_w 1)_{n+1}\, d\Omega_s \\ -\int B_A^T (n^w p_w 1)_{n+1}\, d\Omega_s \\ -\int N_A\, \xi\, (v^s - v^w)_{n+1}\, d\Omega_s \\ \int N_A\, \xi\, (v^s - v^w)_{n+1}\, d\Omega_s \end{bmatrix} \tag{10}$$

$$(f_A^e)_{n+1} = \begin{bmatrix} \int N_A\, \rho^s\, b_{n+1}\, d\Omega_s & \int N_A\, \bar{h}^{s}_{n+1} d\Gamma_h \\ \int N_A\, \rho^w\, b_{n+1}\, d\Omega_s & \int N_A\, \bar{h}^{w}_{n+1} d\Gamma_h \end{bmatrix} \tag{11}$$

where B_A represents the nodal strain displacement matrix and N_A denotes the shape function for the A^{th} node. The quantity $(f_A^i)_{n+1}$ represents the internal forces (both solid and fluid) on node A at time t_{n+1} due to stresses in the soil mass, and $(f_A^e)_{n+1}$ represents the external forces applied to node A at time t_{n+1} due to body force and traction type loads. As long as balance can be achieved between the internal soil stresses and external forces, then the slope will be stable with respect to the applied loads, and the solutions to equation (9) will exist. When this balance can no longer be achieved, however, due to finite soil strength and increased gravity loading, then the slope will become unstable and on the verge of failure, since equilibrium solutions satisfying equation (9) will not exist. In general equation (9) represents a set of nonlinear algebraic equations which must be solved in an iterative fashion for the nodal velocities v_{n+1} at each time step. To obtain updated nodal displacements u_{n+1}, a generalized mid-point rule algorithm is used as

$$u_{n+1} = u_n + (1-\gamma)(\triangle t)_n\, v_n + \gamma(\triangle t)_{n+1}\, v_{n+1} \tag{12}$$

where $\gamma \in [0,1]$ is a constant integration parameter whose value is chosen as unity in the computations presented herein.

The system of global FEM equilibrium equations to be solved at some time $t_{n+1} \in [0, \infty)$ of the problem has the abbreviated form

$$r_{n+1}(v_{n+1}) = 0 \tag{13}$$

Table 1 shows the algorithm sequence to be employed in finding the equilibrium velocity at the $(n+1)^{th}$ time step. In Table 1, K is the global tangent stiffness matrix and δ_k is the line search parameter chosen to satisfy the standard line search criterion. In the linear solving phase represented by equation (14), $K = \frac{dr}{dv}$ can be updated each iteration (pure Newton) or updated only periodically(modified Newton).

2.3 Elastic Consolidation Problem of Porous Medium

When the soil mass is subjected to a stress increase, the pore water pressure is suddenly increased. The excess pore water pressure generated due to loading gradually dissipates over a long period of time (that is, the consolidation). In order to simulate the one-dimensional consolidation behavior, an uniform strip load $p = 1000N/m^2$ over the entire top surface was applied at time $t = 0$, then held constant. Figure 2-a) shows the problem description for one-dimensional porous medium of elastic surface. The total initial height $H = 8m$ and two columns of 16 elements are used. Each element has a side length of $1m$; Young's modulus $E = 1.0 \times 10^7 N/m^2$; Poisson's ratio $\nu = 0.0$; coefficient of consolidation $c_v = 1.0m^2/s$; the solid density $\rho^s = 2.0 \times 10^3 kg/m^3$; the fluid density $\rho^w = 1.0 \times 10^3 kg/m^3$; permeability $k = 9.81 \times 10^{-4} m/s$; porosity $n^w = 0.3$; bulk modulus of fluid $\lambda^w = 2.0 \times 10^9 N/m^2$. The same quadrilateral element were used with four nodes interpolating the displacements field for both solid and fluid. Standard Gaussian quadrature rules were employed in the numerical integration. For the fluid phase the reduced quadrature was used using a $\overline{B}$ procedure. The analytical solution for pore water pressure is available for this problem (Das, 1994). A plot of u versus t is shown in Figure 2-b). Excellent agreement between the numerical and analytical results can be observed.

3. Slope Stability Analysis

3.1 The Limit Strength Analysis Problem

In the proposed analysis method, the time dependent gravitational acceleration vector is prescribed linearly in time by the relation

$$g(t) = g_{baseline} \cdot t \tag{18}$$

where $g_{baseline}$ is a prescribed gravity vector specifying the

Table 1. Global Newton solution algorithm for $(n+1)^{th}$ time step

Predictor Phase		
$k = 0$	: iteration counter initialization	
$v_{n+1}^{(k)} = \tilde{v}_{n+1} = 0$		
$u_{n+1}^{k} = u_n + (1-\gamma)(\triangle t)_{n+1} v_n$	: displacement predictor	
form $r_{n+1}^{k}(v_{n+1}^{k})$	: initial force balance residual	
Multiple Corrector Phase		
while ($\|r_{n+1}^{k}\| > RTOL$)		
$K\delta_k = -r_{n+1}^{k}$	: linear solving phase for δ_k	(14)
$P_k = \alpha_k \delta_k$	: line search to find α_k	(15)
$v_{n+1}^{k+1} = v_{n+1}^{k} + p_k$	: velocity update	(16)
$u_{n+1}^{k+1} = u_{n+1}^{k} + \gamma(\triangle t)_{n+1} p_k$	: displacement update	(17)
form $r_{n+1}^{k+1}(v_{n+1}^{k+1})$	: residual update	
$k = k+1$	: counter update	
end-while		
Go to next time/load step		

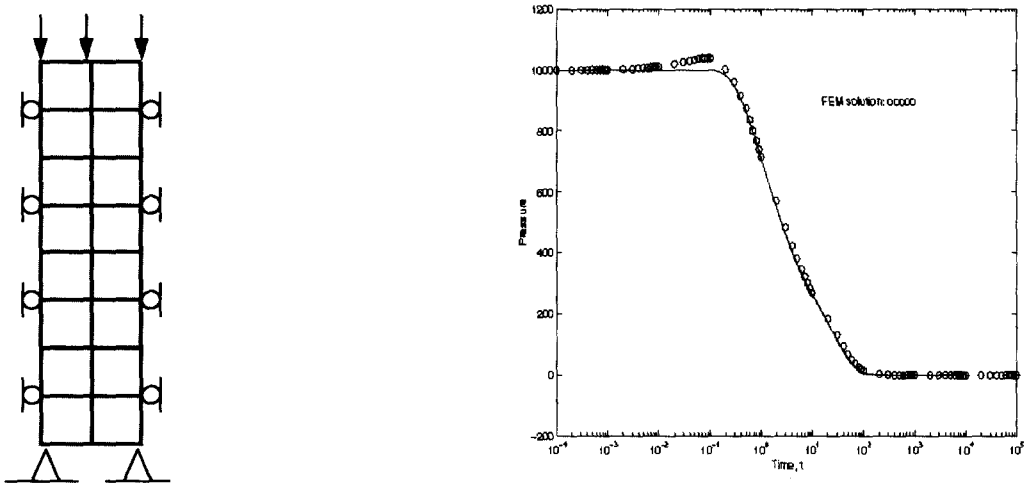

(a) (b)

Fig.2. One-dimensional consolidation geometry and pore pressure at depth 1.5m beneath the load

direction and reference magnitude, and t is a parametric time variable which is assumed to take a value of zero at the inception of the analysis problem. By prescribing the applied gravitational acceleration vector $g(t)$ in this manner, the limit analysis problem reduces simply to finding the largest time $t = t_{\lim}$ for which a global equilibrium solution of Equation (14) exists, and the limiting gravitational acceleration on the system is then merely

$$g_{\lim} = g_{baseline} \cdot t_{\lim} \tag{19}$$

In accordance with the fact that the gravitational loading on slopes is the active agent which induces failure, the proposed new gravity-based factor of safety against failure is simply

$$(FS)_{grav} \equiv \frac{g_{\lim}}{g_{actual}} \tag{20}$$

in which g_{actual} is an appropriate and representative actual gravitational acceleration for the slope being analyzed ($i.e.\ g_{actual} \simeq 9.81 m \cdot s^{-2}$). In general, the higher the computed factor of safety, the more stable a slope is against failure, with values less than unity indicating that a given slope is unstable.

3.2 A Smooth 3-Surface Cap Model

While the proposed slope stability analysis methods described above can be applied with a wide variety of soil plasticity models, they will generally converge more rapidly and produce more meaningful results when used with realistic soil models that feature continuous and smoothly differentiable rate constitutive equations. To efficiently and realistically model coupling between tensile, compressive, and shearing modes of ductile soil plasticity, a smooth, 3-surface cap model (Figure 3) is employed in the calculations that follow in the next section. The model employed here is a smooth variation of the non-smooth cap model originally proposed by DiMaggio and Sandler(1971) and developed for FEM implementation by Simo et al(1988). The primary advantage of the smooth cap model is its continuous differentiability which leads to good convergence behavior in nonlinear limit state FEM computations. In this section, the basic constitutive equations for this relatively simple soil model are briefly discussed.

Utilizing the assumption of small deformations, the strain tensor admits the additive elastic-plastic decomposition

$$\varepsilon = \varepsilon^e + \varepsilon^p \tag{21}$$

where ε, ε^e, ε^p are, respectively, the total, elastic, and plastic strain tensors. The small deformation incremental stress response of the soil is assumed to be related to the strain response by

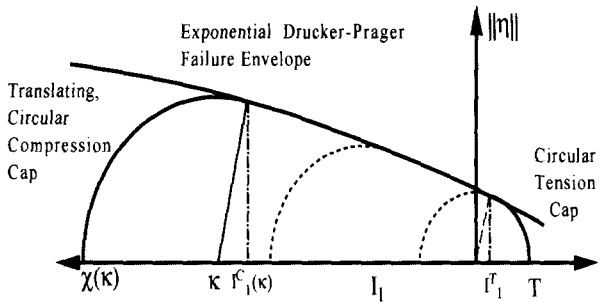

Fig.3. Three surface cap plasticity model

$$\dot{\sigma} = C:(\dot{\varepsilon} - \dot{\varepsilon}^p) \tag{22}$$

where C is a forth order isotropic tensor of elastic moduli $C = K\,1 \otimes 1 + 2\mu\, I_{dev}$ in which K is the bulk modulus of the soil and μ is the shear modulus.

In stress space, the elastic domain is bounded by three distinct but smoothly intersecting yield surfaces. as shown in Figure 3. The mathematical forms are

$$f_1(\sigma) = \| S \| - F_e(I_1) \le 0 \tag{23}$$

$$f_2(\sigma, x) = \| S \|^2 - F_c(I_1, x) \le 0 \tag{24}$$

$$f_3(\sigma) = \| S \|^2 - F_t(I_1) \le 0 \tag{25}$$

where: S is the deviatoric stress tensor and $\|S\|^2 = \frac{1}{2} J_2$; $I_1 \equiv tr(\sigma)$ is the first invariant of the stress tensor and x is an internal variable governing the location of the compressive cap surface and the functional forms of F_e, F_c, F_t are simply

$$F_e(I_1) = \alpha - \lambda(1 - \exp[\beta I_1]) \tag{26}$$

$$F_c(I_1, x) = F_e^2(x) - \left[\frac{I_1 - x}{R}\right]^2 \tag{27}$$

$$F_t(I_1) = T^2 - I_1^2 \tag{28}$$

where the following are material model constants: $\alpha \ge 0$, $\lambda \ge 0$, $\beta \ge 0$ and $R > 0$.

The yield surface $f_1 = 0$ and $f_3 = 0$ depend only on the stress invariant I_1 and $\|s\|$ and thus remain fixed in stress space. In the function F_e the constants θ $(\doteq \lambda\beta)$ and α are related to the Mohr-Coulomb angle of friction ϕ and cohesion c respectively. Approximate translations have been provided as for example in Chen and Saleeb(1982) as

$$\alpha = \frac{\sqrt{2}c}{(1 + 4/3\tan^2\phi)^{1/2}}$$

and $$\theta = \frac{\sqrt{2}\tan\phi}{3(1 + 4/3\tan^2\phi)^{1/2}} \tag{29}$$

The aspect ratio of the elliptical compression cap is provided by the dimensionless constant R. The cap is permitted to translate along the I_1 axis, and in particular moves to the right ($\dot{x} > 0$) during plastic dilatation of the medium, and to the left ($\dot{x} < 0$) during plastic compaction.

The hardening law for this model derives from that the volumetric crush curve is assumed to be an exponential of the form

$$\varepsilon_v^p = -W\{1 - \exp[DX(x)]\} \tag{30}$$

Differentiating equation with respect to x allows us to obtain a variable tangent hardening modulus as follows

$$h'(x) = \frac{d\varepsilon_v^p}{dx} = \frac{\exp(-DX)}{WDX'} \tag{31}$$

where $X(x) = x - RF_e(x)$ and W, D are material constants. This nonlinear hardening modulus $h'(x)$ is used to provide a nonlinear incremental hardening law governing movement of the cap parameter:

$$\dot{x} = h'(x)\ tr(\dot{\varepsilon}^p) \tag{32}$$

The flow rule for this model is associated, and since multiple surfaces are potentially active at any given instant, it takes the form:

$$\dot{\varepsilon}^p = \sum_k \dot{\gamma}^k \frac{\partial f_k}{\partial \sigma} \tag{33}$$

4. Example of Cubzac-les-Point Embankment

This embankment was built for experimental purpose at Cubzac-les-Point, France in 1971. The test embankment program included the construction of the embankment up to failure and calculation of the factor of safety. In 1982, Pilot et al.(1982) analyzed Cubzac embankment by both effective and total stress analyses using simplified Bishop's method. In their analysis, the foundation consisted of a soft silty clay

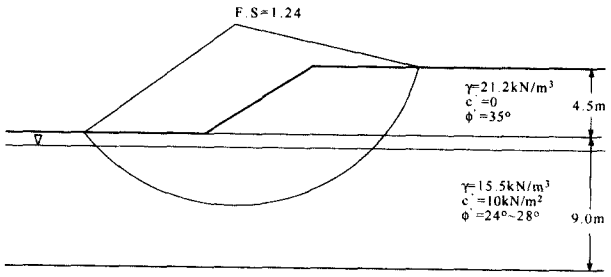

Fig.4. Cubzac Embankment with failure mechanism and factor of safety

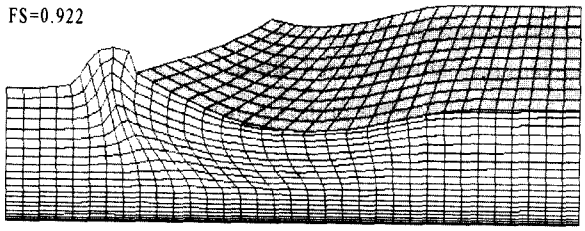

Fig.5. Computed failure mechanism and factor of safety

having an approximate thickness of 9m. The effective shear strength parameters measured by triaxial tests were $c'=10kPa$ and $\phi'=24°\sim28°$. The water table was taken to coincide with the ground level. The embankment material is clean gravel with in situ density of $21.0kN/m^3$; its shear strength parameters were estimated to be $c'=0$ and $\phi'=35°$. The embankment was constructed in approxi- mately 10 days and the failure occurred when the embankment reached a height of 4.5m. Figure 4 shows the test embankment, material properties and the estimated failure surface by Pilot et al along the computed FS of 1.24. For a more detailed description of the embankment, refer to Pilot et al.

The foundation was modeled with clayey soil which has the same thickness and the water table is assumed with the ground surface of the foundation. It also assumed that the foundation is normally consolidated. To simulate the normal consolidation condition, standard gravitational loading was first applied to the foundation until it reach an equilibrium state. The shear strength parameters of the clay were computed by the equation (29). The sand properties λ and β were chosen from Desai's(1981) published data. The compressibility parameters of clayey soil were estimated from those used by Haung and Chen(1990) for Boston Blue Clay. The foundation and embankment material properties are summarized in Table 2. Construction was simulated by gradually increasing gravity loading on the embankment soil until critical failure mechanisms developed. During this time gravity loading on the base soil was held constant. The computed factor of safety and failure mechanism are shown in Figure 5. It should be noted that the computed factor of safety for this embankment is 0.92, where Pilot et al predict a value of 1.24 which would imply a stable embankment.

6. Conclusion

In the slope stability analysis presented, the gravity increase method was applied to simulate the construction of an embankment on a saturated soil deposit. To account for the pore pressure effects, porous medium theory and an elasto-plastic cap model was used. It was found that the coupling between the soil skeletons' shear and compressibility behaviors are very important factors in embankment stabilities. On the demonstrated example of slope stability analysis, an embankment corresponding to a field test

Table 2. Material parameters used for the embankment test

Material Parameter	Values(Foundation)	Value(Embankment)
ρ_d	1600 kg/m^3	2161 kg/m^3
μ	208.3 Mpa	1.154 Gpa
E	500 Mpa	3.0 Gpa
χ_o	0.0 KPa	-10.0 MPa
α	12.3 kPa	10.0 Pa
λ	400.6 KPa	153 kPa
β	5.0×10^{-7} Pa^{-1}	3.48×10^{-6} Pa^{-1}
D	3.2×10^{-7} Pa^{-1}	5.0×10^{-7} Pa^{-1}
W	0.15	0.01

experiment was modeled with the actual construction rate of 10 days. The proposed method is in general agreement with the observed failure in the Cubzac-les-Point field test. The perceived utility of the proposed method is that it facilitates stability analysis of embankments as a function of construction rate by taking into account the in situ soil stresses, the soil shear strength, and the transient effects of pore pressure diffusion.

References

1. Biot, M. A. (1962), "Mechanics of deformation and acoustic propagation in porous media", *J. Appl. Phys.*, 33 pp. 1482-149
2. Borja, R. I. (1986), "Finite element formulation for transient pore pressure dissipation : A variational approach", *Int. J. Solids Struc.*, 22pp. 1201-1211
3. Chen, W.-F. and Saleeb, A. F. (1982), *Constitutive Equations for Engineering Materials, Vol. 1: Elasticity and Modeling*, John-Wiley.
4. Desai, C. S., Phan, H. V., and Sture, S. (1981), "Procedure, selection and application of plasticity model for a soil". *Int. J. Numerical Analysis Methods in Geomech.* 4, pp. 295-311.
5. DiMaggio, F. L. and Sandler, I. S. (1971), "Material models for granlur soils", *J. of Eng. Mech.* ASCE Vol 97. No. EM3 June pp. 935-950
6. Haung, T. K. and Chen, W-F (1990), "Simple procedure for determine cap-plasticity-model parameters", *J. Geotech. Eng.* Vol. 116 No. 3 pp. 492-513
7. Pilot, G., Tark, B., and La Rochelle P. (1982), "Effective stress analysis the stability of embankments on soft soils", *Can. Geotech. J.* 19, pp. 433-450
8. Prevost, J. H. (1980), "Mechanics of continuous porous media", *Int. J. Eng. Sci.* 18, pp. 787-800
9. Simo, J. C., Ju, J-W., Pister K. S. and Taylor, R. L., "Assessment of cap model: consistent return algorithms and rate-dependent extension", *J. Eng. Mech.* 114 No. 2, pp. 191-218
10. Swan, C. C. and Seo, Y-K (1999), "Limit atate analysis of earthern slopes using a continuum/FEM approach" *Int. J. Numerical. Analysis. Methods in Geomech.* 23, pp. 1359-1371
11. Zienkiewicz, O. C., and Shiomi, T., (1984), "Dynamic behavior of saturated porous media the generalized Biot formulation and its numerical solution", *Int. J. Numerical. Anal. Methods Geomech.* 8, pp. 71-96

(접수일자 2001. 1. 30)